Polarizable QM/MM approach with fluctuating charges and fluctuating dipoles: the QM/FQFμ model

Tommaso Giovannini,* Alessandra Puglisi, Matteo Ambrosetti, and Chiara Cappelli*

Scuola Normale Superiore, Piazza dei Cavalieri 7, 56126 Pisa, Italy.

E-mail: tommaso.giovannini@sns.it; chiara.cappelli@sns.it

Abstract

The novel polarizable FQFμ force field is proposed and coupled to a QM SCF Hamiltonian. The peculiarity of the resulting QM/FQFμ approach stands in the fact the polarization effects are modeled in terms of both fluctuating charges and dipoles, which vary as a response to the external electric field/potential. Remarkably, QM/FQFμ is defined in terms of three parameters: electronegativity and chemical hardness, which are well defined in Density Functional Theory, and polarizability, which is a physical observable. Such parameters are numerically adjusted so to reproduce full QM reference electrostatic energy values. The model is challenged against test molecular systems in aqueous solution, showing remarkable accuracy and thus highlighting its potentialities for future extensive applications.

1 Introduction

The problem of describing the interaction between a molecule and its embedding environment is a challenge in Quantum Chemistry. The interplay between the molecule and the environment can in fact dramatically alter both the structure and the electronic response to external electromagnetic fields. The most successful answer to this problem has been found within the realm of multiscale approaches:[1–6] there, the focus is always the molecule and the key is to accurately capture the molecule/environment interactions and their effects on the molecular structure and properties, while neglecting to simulate the intrinsic properties of the environment. Such an approach is based on the assumption that molecular energetic and response properties are local properties of the molecule, which are modified but not determined by the presence of the environment.

In the last years, much effort has been devoted to develop multiscale QM/MM approaches, which keep an atomistic description of all the system under study and are therefore able to model specific molecule-environment interactions, such as hydrogen bonding (HB).[7,8] Most QM/MM approaches developed so far focus on describing the electrostatic interactions between the QM and MM portions. The most physically consistent of such methods are those in which the mutual polarization between the QM and MM portions of the system is recovered. This has led to the development of the so-called polarizable QM/MM approaches, which can be based on distributed multipoles,[9–13] induced dipoles,[14–16] Drude oscillators[17] or Fluctuating Charges (FQ).[18–20] In the latter approach, the electrostatic interaction is described by endowing each MM atom with a charge that can vary as a response to both the differences in electronegativity between MM atoms and in electric potential generated by the QM density.

The classical FQ force field is described only in terms of charges. This poses some conceptual issues because only monopoles, i.e. zeroth order of the electrostatic Taylor expansion, are taken into consideration. As a consequence, the intrinsic anisotropy of some specific molecule-environment interactions, such as HB, is not explicitly taken into account. To overcome this

problem, the electrostatic description of the FQ force field can be refined by including an additional source of polarization. This can be done by adding induced point dipoles,[21] Drude Oscillators (Polarizable Charge Equilibration PQEq),[22,23] or Gaussian-like induced atomic dipoles (Q+P iso $[R, \alpha_{iso}]$ model,[24] Discrete Interaction Model DIM,[25] Capacitance Polarization Model CMM[26]). Differently from the basic formulation of the FQ force field, in the last two approaches gaussian distributions representing the charges, the Drude Oscillators or the induced atomic dipoles are considered, so that the Coulomb law divergence at zero distance, i.e. the so-called "polarization catastrophe", is avoided.[24,25]

In this work, we present a novel polarizable force field, which we will call Fluctuating Charge Fluctuating Dipoles (FQFμ), in which both monopoles (charges) and dipoles can vary as a response to the external Maxwell sources, i.e. electric potential/field. The proposed model founds its fundamental basis on Ref.[24] and overcomes the limitations of FQ at describing anisotripic electrostatic terms. FQFμ is then coupled to a QM description, following the general structure of QM/MM approaches, yielding the novel QM/FQFμ method. Therefore, QM/FQFμ can be seen as a refinement of our previously developed QM/FQ method.[20,27–31]

An important difference between QM/FQFμ (and QM/FQ) and other polarizable QM/MM approaches, is that the latter only adjust the first order of the electrostatic Taylor expansion (i.e. dipole terms) to the QM density, but they keep the monopole (and higher orders) terms fixed. However, it has been proven that charges indeed give the main contribution to the electrostatic interaction energy.[32,33]

As stated before, similar polarizable QM/MM approaches, in which both charges and dipoles are polarizable, have been proposed (see Refs.[25,26]). However, our approach presents several differences with respect to them. The most relevant is that the widths of the gaussian charge/dipoles distributions are defined in terms of atomic chemical hardnesses and polarizabilities, which are the quantities entering the definition of FQFμ. Also, to the best of our knowledge, we report on the first application of a QM/fluctuating charges+fluctuating dipoles approach to molecular systems in a molecular environment (not on surfaces/nanoparticles,

as for instance in Ref.[24–26]). Another relevant novelty of the present work stands in the strategy which is exploited for model parametrization and testing. In fact, parametrization is tuned to get an accurate reproduction of electrostatic interaction energies (vide infra), whereas other approaches rely on atomic parameters defining the specific MM polarizable force field which is actually used.

The manuscript is organized as follows. In the next section, the FQFμ force field is proposed and then coupled to a QM SCF description (QM/FQFμ). A parametrization for aqueous solutions is proposed and applied to the the calculation of electrostatic and total interaction energies of a water dimer as a function of the intermolecular distance. Then, QM/FQFμ is tested against solute-solvent electrostatic interactions of four selected systems in aqueous solution. Some conclusions and future perspectives end the manuscript.

2 Theoretical Model

2.1 FQFμ force field

In the FQFμ force field each MM atom is endowed with both a charge q and an atomic dipole $\boldsymbol{\mu}$, that can vary according to the external electric potential and electric field. Both charges and dipoles are described as s-type gaussian distribution functions:

$$\begin{aligned} \rho_{q_i}(\mathbf{r}) &= \frac{q_i}{\pi^{\frac{3}{2}} R_{q_i}^3} \exp\left(-\frac{|\mathbf{r}-\mathbf{r}_i|^2}{R_q^2}\right) \\ \rho_{\boldsymbol{\mu}_i}(\mathbf{r}) &= \frac{|\boldsymbol{\mu}_i|}{\pi^{\frac{3}{2}} R_{\boldsymbol{\mu}_i}^3} \hat{\mathbf{n}}_i \cdot \boldsymbol{\nabla}\left[\exp\left(-\frac{|\mathbf{r}-\mathbf{r}_i|^2}{R_{\boldsymbol{\mu}_i}^2}\right)\right] \end{aligned} \tag{1}$$

where R_{q_i} and $R_{\boldsymbol{\mu}_i}$ are the width of the Gaussian distributions ρ_{q_i} and $\rho_{\boldsymbol{\mu}_i}$, respectively. $\hat{\mathbf{n}}_i$ is a unit vector pointing to the dipole direction $\boldsymbol{\mu}_i$.

The total energy E associated with a distribution of charges and dipoles is equal to:[24]

$$E(\mathbf{q},\boldsymbol{\mu}) = \sum_i q_i\chi_i + \frac{1}{2}\sum_i q_i\eta_i q_i + \frac{1}{2}\sum_i\sum_{j\neq i} q_i \mathrm{T}_{ij}^{qq} q_j + \sum_i\sum_{j\neq i} q_i \mathbf{T}_{ij}^{q\mu}\boldsymbol{\mu}_j + \\ - \frac{1}{2}\sum_i\sum_{j\neq i}\boldsymbol{\mu}_i^{\dagger}\mathbf{T}_{ij}^{\mu\mu}\boldsymbol{\mu}_j + \frac{1}{2}\sum_i \boldsymbol{\mu}_i^{\dagger}\alpha_i^{-1}\boldsymbol{\mu}_i \tag{2}$$

where χ is the atomic electronegativity, η the chemical hardness and α the atomic polarizability. T_{ij}^{qq}, $\mathbf{T}_{ij}^{q\mu}$ and $\mathbf{T}_{ij}^{\mu\mu}$ are the charge-charge, charge-dipole and dipole-dipole interaction kernels, respectively. If the gaussian distributions in Eq. 1 are adopted, the functional form of the interaction kernels provided by Mayer[24] can be exploited. T_{ij}^{qq} term reads:

$$\mathrm{T}_{ij}^{qq} = \frac{1}{|\mathbf{r}_{ij}|}\mathrm{erf}\left(\frac{|\mathbf{r}_{ij}|}{R_{q_i-q_j}}\right) \tag{3}$$

where $R_{q_i-q_j}$ is equal to $\sqrt{R_{q_i}^2 + R_{q_j}^2}$. When $\mathbf{r}_i$ tends to $\mathbf{r}_j$, the use of gaussian distributions avoids any issues which are related to the typical divergence of Coulomb kernels (i.e. the so-called "polarization catastrophe"):[24,25]

$$\lim_{\mathbf{r}_{ij}\to 0}\mathrm{T}_{ij}^{qq} = \mathrm{T}_{ii}^{qq} = \frac{2}{\sqrt{\pi}}\frac{1}{R_{q_i-q_i}} \tag{4}$$

In order to collect all the quadratic terms in the charges, the diagonal elements of $\mathbf{T}^{qq}$ can be imposed to be equal to the atomic chemical hardnesses η, so that the width of the charge distribution R_q is defined without the need of any parametrization:

$$\mathrm{T}_{ii}^{qq} = \eta_i \Rightarrow R_{q_i} = \sqrt{\frac{2}{\pi}}\frac{1}{\eta_i} \tag{5}$$

where it is assumed $R_{q_i-q_i} = \sqrt{2}R_{q_i}$.

The charge-dipole and dipole-dipole interaction kernels are obtained as first and second derivatives of the charge-charge interaction kernel in Eq. 3:[24]

$$\mathbf{T}_{ij}^{q\mu} = -\boldsymbol{\nabla}_{r_i} \mathrm{T}_{ij}^{qq} = -\frac{\mathbf{r}_{ij}}{|\mathbf{r}_{ij}|^3}\left[\mathrm{erf}\left(\frac{|\mathbf{r}_{ij}|}{R_{q_i-\mu_j}}\right) - \frac{2|\mathbf{r}_{ij}|}{\sqrt{\pi}R_{q_i-\mu_j}}\exp\left(\frac{-|\mathbf{r}_{ij}|}{R_{q_i-\mu_j}}\right)^2\right] \tag{6}$$

$$\mathbf{T}_{ij}^{\mu\mu} = \boldsymbol{\nabla}_{r_j} \mathbf{T}_{ij}^{q\mu} = \frac{3\mathbf{r}_{i,j}\otimes\mathbf{r}_{i,j} - |\mathbf{r}_{i,j}|^2\mathbf{I}}{|\mathbf{r}_{i,j}|^5}\left[\mathrm{erf}\left(\frac{|\mathbf{r}_{ij}|}{R_{\mu_i-\mu_j}}\right) - \frac{2}{\sqrt{\pi}}\frac{|\mathbf{r}_{ij}|}{R_{\mu_i-\mu_j}}\exp\left(-\frac{\mathbf{r}_{ij}}{R_{\mu_i-\mu_j}}\right)^2\right] + \\ - \frac{4}{\sqrt{\pi}R_{\mu_i-\mu_j}^3}\frac{\mathbf{r}_{ij}\otimes\mathbf{r}_{ij}}{|\mathbf{r}_{ij}|^2}\exp\left(-\frac{|\mathbf{r}_{ij}|}{R_{\mu_i-\mu_j}}\right)^2 \tag{7}$$

where $R_{x_i-x_j} = \sqrt{R_{x_i}^2 + R_{x_j}^2}(x = q, \mu)$ and $\mathbf{I}$ is the identity matrix. Similarly to what was done before for T_{ij}^{qq}, the limits for $\mathbf{r}_{ij} \to 0$ in the case of $\mathbf{T}_{ij}^{q\mu}$ and $\mathbf{T}_{ij}^{\mu\mu}$ are:

$$\lim_{\mathbf{r}_{ij}\to 0} \mathbf{T}_{ij}^{q\mu} = \mathbf{T}_{ii}^{q\mu} = 0 \tag{8}$$

$$\lim_{\mathbf{r}_{ij}\to 0} \mathbf{T}_{ij}^{\mu\mu} = \mathbf{T}_{ii}^{\mu\mu} = -\sqrt{\frac{2}{\pi}}\frac{\mathbf{I}}{3R_{\mu_i}^3} \tag{9}$$

From Eq.9, R_{μ_i} can be defined in terms of the atomic polarizability α_i:

$$\alpha_i^{-1} = \sqrt{\frac{2}{\pi}}\frac{1}{3}\frac{1}{R_{\mu_i}^3} \Rightarrow R_{\mu_i} = \left(\sqrt{\frac{2}{\pi}}\frac{1}{3}\alpha_i\right)^{\frac{1}{3}} \tag{10}$$

The definition of the gaussian width R_{q_i} and R_{μ_i} in terms of η_i and α_i limits the number of parameters which enter the definition of FQFμ to electronegativity, chemical hardness and polarizability for each atom type. Therefore, Eq. 2 can be formally rewritten as:

$$E(\mathbf{q}, \boldsymbol{\mu}) = \frac{1}{2}\sum_i\sum_j q_i \mathrm{T}_{ij}^{qq} q_j + \frac{1}{2}\sum_i\sum_j \boldsymbol{\mu}_i^\dagger \mathbf{T}_{ij}^{\mu\mu}\boldsymbol{\mu}_j + \sum_i\sum_j q_i \mathbf{T}_{ij}^{q\mu}\boldsymbol{\mu}_j^\dagger + \sum_i q_i\chi_i = \\ = \frac{1}{2}\mathbf{q}^\dagger\mathbf{T}^{qq}\mathbf{q} + \frac{1}{2}\boldsymbol{\mu}^\dagger\mathbf{T}^{\mu\mu}\boldsymbol{\mu} + \mathbf{q}^\dagger\mathbf{T}^{q\mu}\boldsymbol{\mu} + \boldsymbol{\chi}^\dagger\mathbf{q} \tag{11}$$

where a matrix notation has been adopted. Notice that FQFμ can be further expanded to consider also polarizable quadrupolar terms, by only defining the appropriate interaction kernels.

In Eq. 11, the sum of charge values is not forced by any external constrain. However, the equilibrium condition is reached when the Electronegativity Equalization Principle (EEP) is satisfied. Such a principle states that at equilibrium each atom has the same electronegativity. Thus, an energy functional to be minimized can be written for instance by adopting Lagrangian multipliers. Notice that we can in principle assume:

- The entire system is constrained to have charge $\mathrm{Q_{tot}}$, and no constraint is imposed on single molecules. This permits inter-molecular Charge Transfer (CT) and makes, at the equilibrium, the electronegativity of each atom to be the same.

- Each molecule is constrained to assume a fixed, total charge Q_α, which sums to $\mathrm{Q_{tot}}$). Therefore, the electronegativity of each atom in the same molecule is the same but generally has different values among different molecules.

We report here the equations obtained by adopting the first assumption. Consistently with what has been done for FQ by some of the present authors,[28,34] similar equations can be derived under the second assumption : they are given in Section S1 of the Supporting Information (SI). Notice that our implementation is general and can treat both cases. The energy functional F can be written by exploiting the Lagrangian multiplier (λ):

$$
\begin{aligned}
F\left(\mathbf{q},\boldsymbol{\mu},\lambda\right) &= E\left(\mathbf{r},\mathbf{q},\boldsymbol{\mu}\right) + \lambda\left[\sum_i\left(q_i\right) - Q_{\mathrm{tot}}\right] = \\
&= \frac{1}{2}\sum_i\sum_j q_i \mathrm{T}_{ij}^{qq} q_j + \frac{1}{2}\sum_i\sum_j \boldsymbol{\mu}_i^\dagger \mathbf{T}_{ij}^{\mu\mu}\boldsymbol{\mu}_j + \sum_i\sum_j q_i \mathbf{T}_{ij}^{q\mu}\boldsymbol{\mu}_j^\dagger + \sum_i q_i\chi_i \\
&+ \lambda\left[\sum_i\left(q_i\right) - Q_{\mathrm{tot}}\right] = \\
&= \frac{1}{2}\mathbf{q}^\dagger\mathbf{T}^{qq}\mathbf{q} + \frac{1}{2}\boldsymbol{\mu}^\dagger\mathbf{T}^{\mu\mu}\boldsymbol{\mu} + \mathbf{q}^\dagger\mathbf{T}^{q\mu}\boldsymbol{\mu} + \boldsymbol{\chi}^\dagger\mathbf{q} + \lambda\mathbf{q}
\end{aligned}
\tag{12}
$$

where λ is meant to preserve the total charge Q_{tot} of the MM portion. Therefore, the conditions for the constrained minimum are found by imposing the derivatives of F with respect to all the variables to be zero, resulting in the following linear problem:

$$\begin{cases} \sum_j \mathbf{T}^{qq}_{i,j} q_j + \lambda + \sum_j \mathbf{T}^{q\mu}_{i,j} \boldsymbol{\mu}_j = -\chi_i \\ \sum_j \mathbf{T}^{\mu\mu}_{i,j} \boldsymbol{\mu}_j + \sum_j \mathbf{T}^{q\mu}_{i,j} q_j = 0 \\ \sum_i q_i = Q_{\text{tot}} \end{cases} \tag{13}$$

The whole system can be recast in a more compact form as:[21,26]

$$\begin{pmatrix} \mathbf{T}^{qq} & \mathbf{1}_\lambda & \mathbf{T}^{q\mu} \\ \mathbf{1}_\lambda^\dagger & 0 & \mathbf{0} \\ -\mathbf{T}^{q\mu^\dagger} & \mathbf{0} & \mathbf{T}^{\mu\mu} \end{pmatrix} \begin{pmatrix} \mathbf{q} \\ \lambda \\ \boldsymbol{\mu} \end{pmatrix} = \begin{pmatrix} -\boldsymbol{\chi} \\ Q_{\text{tot}} \\ \mathbf{0} \end{pmatrix} \quad \Rightarrow \quad \mathbf{D}\mathbf{Q}_\lambda = -\mathbf{C}_Q \tag{14}$$

where $\mathbf{1}_\lambda$ is a vector which accounts for the Lagrangian. $\mathbf{C}_Q$ is a vector containing atomic electronegativities and total charge constraint, whereas $\mathbf{Q}_\lambda$ is a vector containing charges, dipoles and the Lagrange multiplier.

2.2 The QM/FQFμ model

In order to couple FQFμ to a QM wavefunction in a QM/MM framework, the first step is to define an extended energy functional, which is composed of three terms:

$$\mathcal{E} = E_{QM} + E_{MM} + E_{QM/MM} \tag{15}$$

where E_{MM} is defined in Eq. 12. If the QM term is a variational functional itself, the resulting, coupled equations are derived following the same procedure as for the uncoupled case. The QM density interacts as a classical density of charge with both charges and dipoles:

$$E_{QM/MM} = \sum_i V[\rho_{QM}](\mathbf{r}_i) q_i - \boldsymbol{\mu}_i^\dagger \mathbf{E}[\rho_{QM}](\mathbf{r}_i) \tag{16}$$

where $V[\rho_{QM}](\mathbf{r}_i)$ and $\mathbf{E}[\rho_{QM}](\mathbf{r}_i)$ are the electric potential and electric field, respectively, calculated at the i-th charge and i-th dipoles placed at $\mathbf{r}_i$. The QM potential and the electric field are composed by an electronic ($\mathbf{V}^e$, $\mathbf{E}^e$) and a nuclear ($\mathbf{V}^N$, $\mathbf{E}^N$) contribution:

$$V[\rho_{QM}](\mathbf{r}_i) = V_i[\mathbf{P}] = V_i^N(\mathbf{P}) + V_i^e(\mathbf{P}) = \sum_\zeta \frac{Z_\zeta}{|\mathbf{r}_i - \mathbf{R}_\zeta|} + \int_{\mathbb{R}^3} \frac{\rho_{el}(\mathbf{r})}{|\mathbf{r}_i - \mathbf{r}|}\, \mathrm{d}\mathbf{r} \tag{17}$$

$$\mathbf{E}[\rho_{QM}](\mathbf{r}_i) = \mathbf{E}_i(\mathbf{P}) = \mathbf{E}_i^N(\mathbf{P}) + \mathbf{E}_i^e(\mathbf{P}) = \sum_\zeta \frac{Z_\zeta(\mathbf{R}_\zeta - \mathbf{r}_i)}{|\mathbf{r}_i - \mathbf{R}_\zeta|^3} - \int_{\mathbb{R}^3} \frac{\rho_{el}(\mathbf{r})(\mathbf{r}_i - \mathbf{r})}{|\mathbf{r}_i - \mathbf{r}|^3}\, \mathrm{d}\mathbf{r} \tag{18}$$

where ρ_{el} is the electron density. ζ index runs over the QM nuclei, whose charges are named Z_ζ and whose positions are $\mathbf{R}_\zeta$. If the electronic density $\rho_{el}(\mathbf{r})$ is expanded in an atomic basis set $\{\chi_\mu\}$, the second terms in Eqs.17 and 18 become:

$$V_i^e(\mathbf{P}) = -\sum_{\nu\mu} P_{\mu\nu} \int_{\mathbb{R}^3} \mathrm{d}\mathbf{r} \frac{\chi_\mu(\mathbf{r})\chi_\nu(\mathbf{r})}{|\mathbf{r}_i - \mathbf{r}|} = \sum_{\mu\nu} P_{\mu\nu} V_{\mu\nu,i} \tag{19}$$

$$\mathbf{E}_i^e(\mathbf{P}) = -\sum_{\mu\nu} P_{\mu\nu} \int_{\mathbb{R}^3} \frac{\chi_\mu(\mathbf{r})\chi_\nu(\mathbf{r})(\mathbf{r}_i - \mathbf{r})}{|\mathbf{r}_i - \mathbf{r}|^3} = \sum_{\mu\nu} P_{\mu\nu} E_{\mu\nu,i} \tag{20}$$

where we have introduced the "uncontracted" potential $V_{\mu\nu}$ and the "uncontracted" field $E_{\mu\nu}$. $P_{\mu\nu}$ are elements of the QM density matrix. Finally, the global QM/MM energy functional for a SCF-like description of the QM portion is:

$$\begin{aligned} F(\mathbf{P}, \mathbf{q}, \boldsymbol{\mu}, \boldsymbol{\lambda}) = \mathrm{tr}\mathbf{h}\mathbf{P} + \frac{\mathbf{1}}{\mathbf{2}}\mathrm{tr}\mathbf{P}\mathbf{G}(\mathbf{P}) + \frac{\mathbf{1}}{\mathbf{2}}\mathbf{q}^\dagger\mathbf{T}^{\mathbf{qq}}\mathbf{q} + \frac{\mathbf{1}}{\mathbf{2}}\boldsymbol{\mu}^\dagger\mathbf{T}^{\mu\mu}\boldsymbol{\mu} + \mathbf{q}^\dagger\mathbf{T}^{\mathbf{q}\mu}\boldsymbol{\mu} + \boldsymbol{\chi}^\dagger\mathbf{q} + \boldsymbol{\lambda}^\dagger\mathbf{q} + \\ + \mathbf{q}^\dagger\mathbf{V}(\mathbf{P}) - \boldsymbol{\mu}^\dagger\mathbf{E}(\mathbf{P}) \end{aligned} \tag{21}$$

where

$$h_{\mu\nu} = \langle\psi_\mu| - \frac{\nabla^2}{2} - \sum_\zeta \frac{Z_\zeta}{|\mathbf{r} - \mathbf{R}_\zeta|}|\psi_\nu\rangle$$

$$G_{\mu\nu} = \sum_{\sigma\tau} P_{\sigma\tau} \left(\langle\mu\sigma|\nu\tau\rangle - c_x\langle\mu\sigma|\tau\nu\rangle\right) + c_l\langle\psi_\mu|v^{xc}|\psi_\nu\rangle$$

are the usual one- and two-electron matrices. The coefficients c_x and c_l define whether Hartree–Fock ($c_x = 1, c_l = 0$), pure DFT ($c_x = 0, c_l = 1$), or hybrid DFT are exploited. For the sake of brevity, we will refer to both the HF and KS matrices as Fock matrix. The effective Fock matrix is defined as the derivative of the energy with respect to the density matrix:

$$\tilde{F}_{\mu\nu} = \frac{\partial\mathcal{E}}{\partial P_{\mu\nu}} = h_{\mu\nu} + G_{\mu\nu}(\mathbf{P}) + \mathbf{V}^\dagger_{\mu\nu}\mathbf{q} - \mathbf{E}^\dagger_{\mu\nu}\boldsymbol{\mu} \tag{22}$$

where the interaction of the electron density with both charges and dipoles are included through the coupling electrostatic terms. Charges and dipoles are obtained by imposing the global functional to be stationary with respect to charges, dipoles and Lagrangian multiplier.

$$\begin{pmatrix} \mathbf{T}^{qq} & \mathbf{1}_\lambda & \mathbf{T}^{q\mu} \\ \mathbf{1}^\dagger_\lambda & 0 & \mathbf{0} \\ -\mathbf{T}^{q\mu^\dagger} & \mathbf{0} & \mathbf{T}^{\mu\mu} \end{pmatrix} \begin{pmatrix} \mathbf{q} \\ \lambda \\ \boldsymbol{\mu} \end{pmatrix} = \begin{pmatrix} -\boldsymbol{\chi} \\ Q_{\text{tot}} \\ \mathbf{0} \end{pmatrix} + \begin{pmatrix} -\mathbf{V}(\mathbf{P}) \\ 0 \\ \mathbf{E}(\mathbf{P}) \end{pmatrix} \qquad \Rightarrow \qquad \mathbf{D}\mathbf{Q}_\lambda = -\mathbf{C}_Q - \mathbf{S}(\mathbf{P}) \tag{23}$$

Notice that, with respect to Eq. 14, a new source term $\mathbf{S}(\mathbf{P})$ arises. Such a term, which represents the coupling of both charges and dipoles with the SCF density, permits to determine them for a given density matrix.

QM/FQFμ introduces two polarization sources: fluctuating charges and fluctuating dipoles. From Eq. 23 both QM/FQ and QM/Induced Dipoles can be recovered by considering only charge-charge or dipole-dipole blocks in the linear system. QM/FQFμ response matrix is four times bigger than the QM/FQ one (T^{qq} block). As a consequence, QM/FQ can treat four times bigger systems than QM/FQFμ at the same computational cost. Similarly to

QM/Induced Dipoles, QM/FQFμ introduces two contributions in Fock matrix (see Eq. 22). However, in QM/FQFμ both the zeroth order monopoles and the first order dipoles are indeed dependent on the QM density. This only causes a small increase in the computational cost with respect to QM/Induced Dipoles, because the response matrix need to be enlarged so to include the T^{qq} block (which is squared the number of MM atoms).

As pointed out in the Introduction, QM/FQFμ finds its fundamentals in Ref.,[24] similarly to QM/DIM[35] and QM/CMM.[26] However, the definition of the gaussian widths, which in both QM/DIM and QM/CMM are external parameters, is automatically obtained in QM/FQFμ from chemical hardnesses and polarizabilities (see Eqs. 5 and 10). As a consequence, QM/FQFμ is defined only in terms of three parameters for each atom type: electronegativity, chemical hardness and polarizability. A second relevant difference stands in the formulation of the interaction between QM and MM portions. In QM/CMM, the electrostatic interactions is expressed in terms of a Coulomb integral of the gaussian distributions of both charges and dipoles with the QM density.[26] In this way, Coulomb repulsion is also taken into account. In QM/FQFμ, instead, MM charges and dipoles are seen as point charges and point dipoles by the QM density, as it is generally assumed in most polarizable QM/MM approaches. However, QM/FQFμ can be reformulated in a similar way to QM/DIM and QM/CMM, for instance by following what has been proposed in other contexts.[36] In addition, differently from DIM and CMM, FQFμ has been formulated in terms of a variational functional (see Eqs. 12 and 21), which guarantees its rigorous further extension to molecular properties.[37] It is worth remarking that the application of both QM/DIM and QM/CMM has been so far limited to the study of molecular properties of systems adsorbed on a metal surface, in which the metal surface is described by DIM or CMM force fields.[38–41] The heterogeneous environment is instead modeled in terms of non-polarizable force fields.[38] QM/FQFμ is not limited to any specific kind of environment (pending an accurate parametrization is obtained), thus being of broader applicability with respect to other approaches.

2.3 Fluctuating Dipoles vs Drude Oscillators

FQFμ describes the first order of electrostatic Taylor expansion in terms of fluctuating dipoles. As an alternative, Drude oscillators can be employed, as it has been recently proposed in the PQEq force field.[22] PQEq combines the Charge Equilibration model (QEq)[42] with the Drude Oscillator approach.[43] Each MM atom is seen as composed of a core and a shell, on which gaussian charge distributions are placed. In particular, both a fluctuating charge (q) and a fixed charge ($+Z$) are placed on the core. The fixed charge is connected trough an isotropic harmonic spring to the shell fixed but mobile charge ($-Z$), thus allowing variable charge displacements. PQEq can be coupled to a QM description by following the same strategy adopted above for QM/FQFμ, yielding the QM/PQEq model. In this approach fluctuating charges result from the solution of a modified FQ system, whereas the positions of the shell mobile charges are obtained by imposing the total electric force acting on them to be zero (see Section S2, given as SI). QM/PQEq Fock operator reads:

$$\tilde{F}_{\mu\nu} = \frac{\partial \mathcal{E}}{\partial P_{\mu\nu}} = h_{\mu\nu} + G_{\mu\nu}(\mathbf{P}) + \mathbf{V}^{\dagger}_{\mu\nu,c}\mathbf{q} + \mathbf{V}^{\dagger}_{\mu\nu,c}\mathbf{Z} - \mathbf{V}^{\dagger}_{\mu\nu,s}\mathbf{Z} \tag{24}$$

where, $\mathbf{q}$ and $\mathbf{Z}$ are the vectors containing fluctuating and fixed charges, respectively, whereas c and s subscripts indicate core and shell positions, where the QM potential $\mathbf{V}$ is calculated. Thus, differently from QM/FQFμ, QM/PQEq is defined only in terms of the QM electric potential. The equation which defines the equilibrium positions of shell mobile charges (see Eq. S11 given as SI) introduces a non-linearity in the problem, which can be solved only by exploiting iterative techniques.[17,44–46] Also, due to its non-linearity, QM/PQEq could present some issues in the definition of the response property of the QM portion. On the contrary, this does not apply to QM/FQFμ. Due to its linearity and variational nature, QM/FQFμ can be extended to the calculation of molecular properties[12,28,29,47–51] by using the standard techniques of quantum chemistry.[52] PQEq can indeed be mapped into the FQFμ approach, similarly to what has been done in the case of basic Drude Oscillator and

Induced Dipole force fields.[53]

3 Computational Details

QM/FQFμ was implemented in a locally modified version of Gaussian16.[54] All QM/FQ and QM/FQFμ calculations were performed by treating the QM portion at the HF or DFT levels of theory, combined with selected basis sets. Three different parametrizations to treat the FQ electrostatic component in QM/FQ calculations were exploited, taken from ref.,[18] ref.[49] and ref.[55] Non-electrostatic contributions, i.e. repulsion and dispersion, were modeled as reported in Ref.[56] All the classical Molecular Dynamics (MD) simulations were performed with the Gromacs package,[57–60] by keeping the same settings as previously reported by some of the present authors.[27,61,62] Details on MD simulations are given as SI. The Kitaura-Morokuma Energy Decomposition Analysis (KM-EDA)[63,64] was performed by using the GAMESS package.[65,66] Symmetry Adapted Perturbation Theory (SAPT)[67,68] calculations were performed by using Psi4 1.1.[69]

4 Numerical Results

In this section, the parametrization of the QM/FQFμ approach to treat aqueous solutions is presented and discussed. Then, the resulting parameters are tested to reproduce electrostatic energies of a water dimer as a function of the oxygen-oxygen distance as computed at the KM-EDA/6-31+G* level. Then, the total interaction energy E_{int}, i.e. the sum of electrostatic (E_{ele}), repulsion (E_{rep}) and dispersion (E_{dis}) contributions, is compared to SAPT2+3(CCD)/aug-cc-pVTZ and CCSD(T)/aug-cc-pVTZ with Counter-Poise corrections values for the same dimer. The dependence of the QM/FQFμ electrostatic energy on the level of theory, i.e. the combination of HF/DFT with several basis sets is also discussed. Finally, in order to test the transferability of our parameters to other systems, four molecules (Methyloxirane, Acrolein, N-Methyl Acetamide and Methanol) in aqueous solu-

tion are studied. In such cases, QM/FQFμ and QM/FQ electrostatic energies are compared to SAPT0/6-311++G** values.

4.1 Model Parametrization

QM/FQFμ is general enough to model any kind of external environment, pending an appropriate parametrization of the quantities entering Eqs. 21 and 22. Such a parametrization is a crucial step towards the routinely application of the method to real cases. In this section we will focus on aqueous solutions, which will also allow for a quantitative comparison with QM/FQ, thus highlighting the effect of including atomic fluctuating dipoles in QM/MM electrostatic energies.

In order to set the parameters entering Eq. 21, selected water clusters taken from Kratz et al.[70] (see Figure 1), were studied. Reference full QM electrostatic energy values of such clusters were calculated by performing a KM-EDA[63,64] calculation on each structure in Figure 1 at the HF/6-31+G* level, according to what has already been proposed in the literature.[56,71,72]

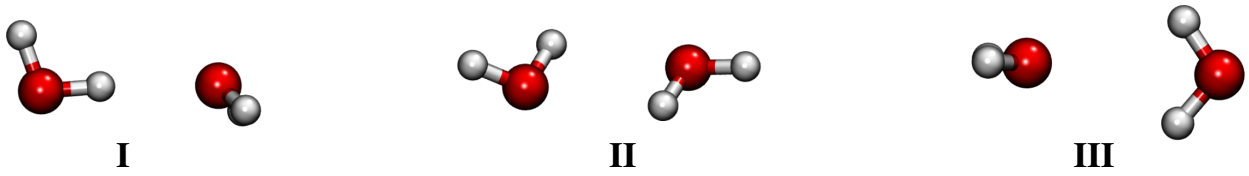

Figure 1: Structures of water dimers exploited in the parametrization of QM/FQFμ.

KM-EDA values were compared to electrostatic energies obtained with the QM/FQFμ model. In the latter, one water molecule was treated at the QM level (HF/6-31+G*), whereas the second molecules was described by means of the FQFμ force field. For each dimer structure two calculations were performed, by exchanging the QM and FQFμ water molecules. Remarkably, electrostatic interaction is by definition symmetric if the two water molecules are interchanged. Thus, differently to what some of the present authors reported for the parametrization of non-electrostatic contributions,[56] we imposed the two calculations (i.e.

the MM water molecule acts as HB donor or acceptor) to give the same results. In such a way the transferability of the final parameters should be guaranteed. Notice that in the QM/FQFμ approach, electrostatic and polarization terms cannot be separated, because the electrostatic charge contribution is partially due to QM polarization (see Eq. 23). Thus, QM/FQFμ electrostatic energies are compared with the sum of electrostatic and polarization KM-EDA energy contributions.

For the studied dimers, Eq. 21 depends on six parameters (electronegativities, chemical hardnesses and polarizabilities of hydrogen and oxygen atoms, respectively): their best values were defined by performing a least square roots fitting on full KM-EDA data, by allowing the parameters to vary freely. Their best fitted values are reported in Table S1 in the SI. Electrostatic energies of the selected water dimers are reported in Table S2 in SI. The reliability of the parametrization protocol is confirmed by the agreement between QM/FQFμ and KM-EDA data. The effects due to the introduction of atomic dipoles can also be quantified. The zeroth order monopoles, i.e. fluctuating charges, account for almost 70$\sim$72 % of the total electrostatic energy, whereas the first order dipoles for 28$\sim$30%, i.e. they give a minor, but not negligible contribution.

4.2 Interaction energy of a water dimer as a function of O-O distance

In this section, the dependence of E_{ele} and E_{int} on the water-water intermolecular distance is investigated. To this end, the water dimer depicted in Figure 2 (optimized at the MP2/aug-cc-pVQZ level) was exploited, and the distance d between the oxygen atoms was taken as reference.

In Figure 3, QM/FQFμ E_{ele} is reported as a function of d. The plot was constructed by increasing the O-O distance from 2.54 Å to 6.49 Å by a step of 0.05 Å (80 points). E_{ele} was calculated by treating the QM moiety at the HF/6-31+G* level. Again, QM and MM moieties were interchanged, and the average values were taken. Charge and dipole

Figure 2: Structure of the water dimer used to study the dependence of electrostatic and interaction energies as a function of O-O intermolecular distance.

electrostatic contributions QM/FQF$\mu|_q$ and QM/FQF$\mu|_\mu$, are also depicted, showing that also in this case the charge contribution is dominating at all distances (70 $\sim$ 72 %).

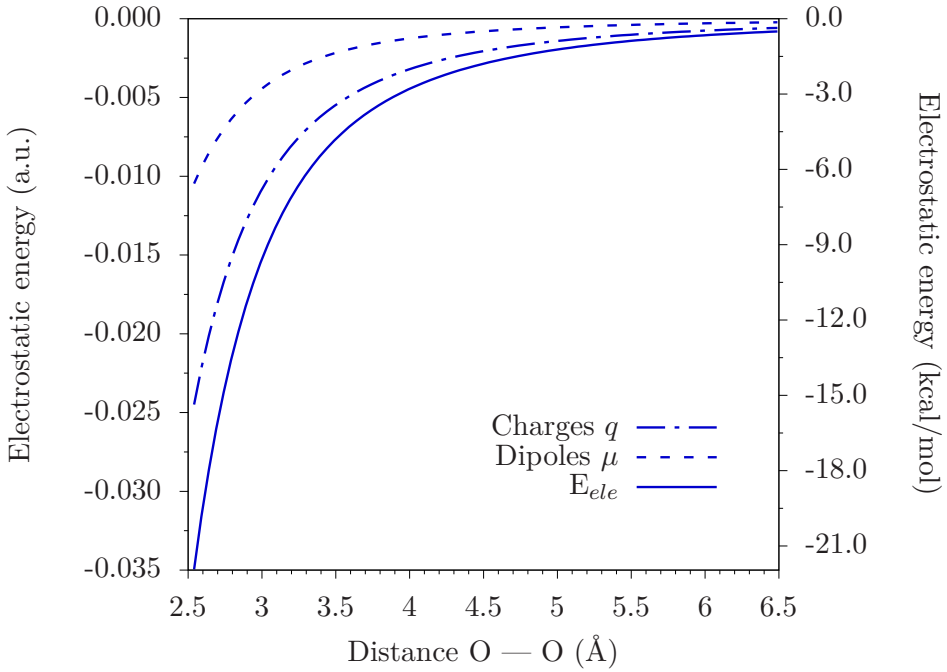

Figure 3: Plot of the QM/FQFμ electrostatic energy as a function of the O-O intermolecular distance for the water dimer depicted in Figure 2. Charge and dipole contributions to E$_e$*le* are also plotted.

In Figure 4, computed QM/FQFμ electrostatic energies are compared with KM-EDA full-QM reference electrostatic (summed with polarization) energies. An almost perfect superposition is observed, the average computed error being of about 7% and the computed Root Mean Squared Deviation (RMSD) being only 0.29 kcal/mol ($\sim$ 0.47 mH). The excellent reproduction of E$_{ele}$ is not unexpected, because the dimer structure under study is very similar to structure **I** exploited in the parametrization step (see Fig.1).

The inset in Figure 4 shows the difference between calculated QM/FQFμ E_{ele} values obtained by assuming the QM water molecule to act as H-bond donor or acceptor.The two curves are almost superimposed, as expected by considering the parametrization protocol that we have followed (see previous section).

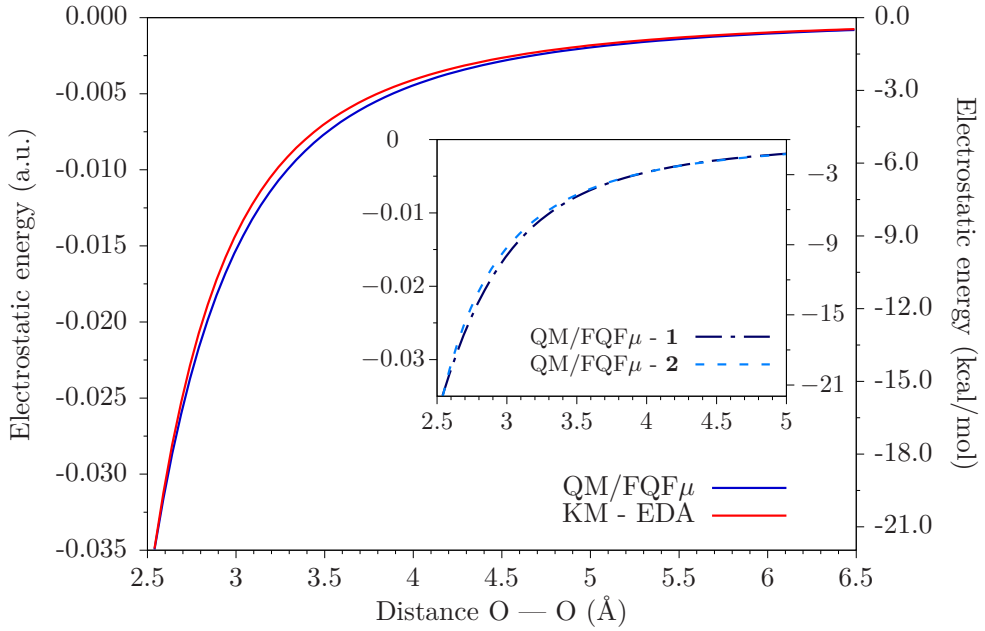

Figure 4: Plot of the electrostatic energy as a function of the O-O intermolecular distance for the water dimer depicted in Figure 2. QM/FQFμ values (HF/6-31+G* for the QM moiety) are compared to KM-EDA (HF/6-31+G*) calculations. In KM-EDA calculations, electrostatic and polarization contributions are summed up. In the inset QM/FQFμ E_{ele} as a function of the O-O distance is depicted for the two structures (**1** and **2**) in Figure 2.

To end this discussion, the total B3LYP/aug-cc-pVTZ QM/FQFμ interaction energy as a function of d is plotted in Figure 5 and compared with SAPT2+3(CCD)/aug-cc-pVTZ or CCSD(T)/aug-cc-pVTZ data (counterpoise corrections are included). To this end, QM/FQFμ is coupled to the approach proposed by some of the present authors to model non-electrostatic repulsion/dispersion contributions,[56] which formulates repulsion in terms of an auxiliary density on the MM portion, whereas QM/MM dispersion is obtained by extending the Tkatchenko-Scheffler approach to DFT.[73–77]

Clearly, QM/FQFμ+dis/rep is able to correctly reproduce both CCSD(T) equilibrium distance (2.99 Å vs. 2.99 Å) and CCSD(T) interaction energy at the equilibrium distance

(-4.56 vs. -4.65 kcal/mol). The RMSD calculated over all 80 structures is 0.34 kcal/mol.

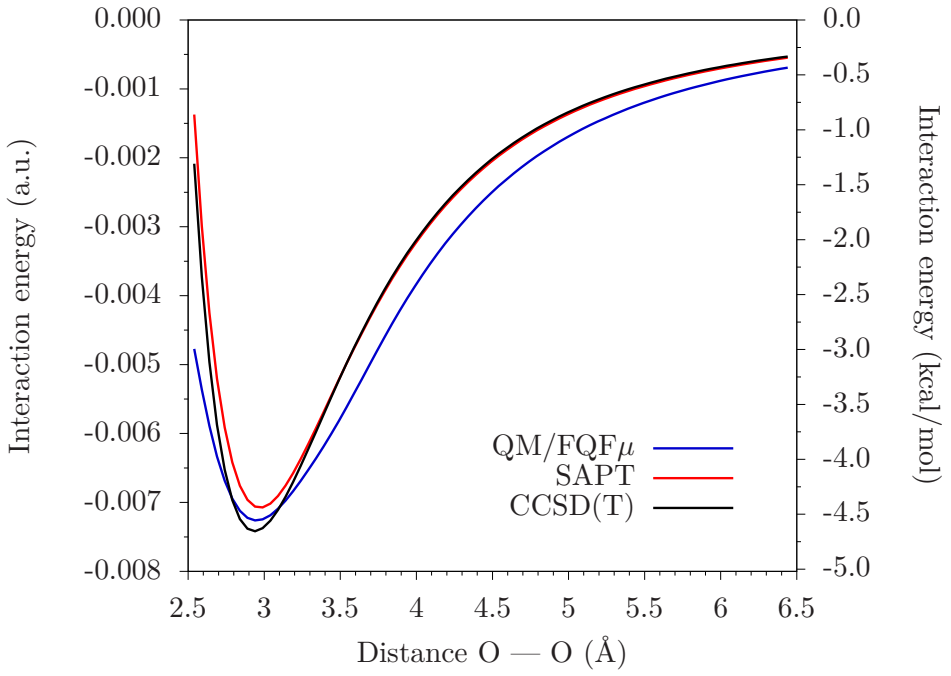

Figure 5: QM/FQFμ (B3LYP/aug-cc-pVTZ for the QM moiety), SAPT2+3(CCD) and CCSD(T)/aug-cc-pVTZ total interaction energies for the water dimer in Figure 2 as a function of the O-O distance.

4.3 Dependence on the QM level of theory

In this section, the dependence of calculated QM/FQFμ E_{ele} values on the level used to model the QM moiety is studied. To this end, the water dimer depicted in Figure 2 with $d = 2.94$ Å is exploited. Thirteen different methods were used by following the recent literature,[78,79] ranging from HF to pure DFT functionals (LDA, PBE,[80] B97D,[81,82] R-TPSS[83]), to different classes of hybrid functionals (BLYP,[84] M06,[85] PBE0,[86] B3LYP,[87] M062X,[85] SOGGA11-X,[88] mPW1PW91[89]), also including long-range (CAM-B3LYP[90]). Each functional was coupled to several Pople-type basis sets (see Figure 6), in order to separate the contributions arising from polarization and diffuse functions. In addition, correlation-consistent and augmented correlation-consistent basis sets were employed, up to aug-cc-pVQZ.[91]

Figure 6 schematically reports the observed trends. Numerical values are given in Table S3

in the SI.

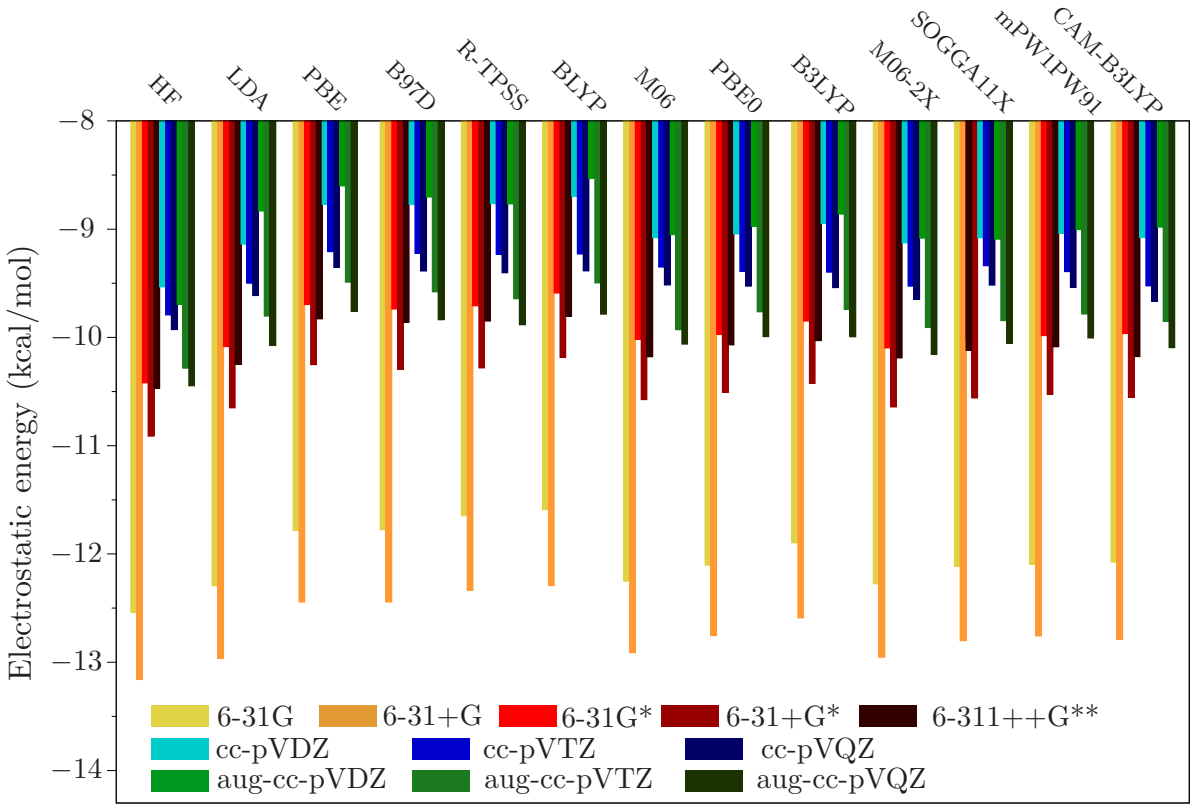

Figure 6: Dependence of E_{ele} on the choice of basis set and QM method for the water dimer depicted in Figure 2 with $d = 2.94$ Å.

All employed QM methods predict very similar E_{ele} values as varying the basis set, with HF always showing the highest absolute values for a given basis set (on average, HF values are about 5% higher than the absolute average value of the other methods). The lowest absolute values are instead shown by PBE and BLYP functionals. However, the difference between HF and PBE/BLYP functionals (i.e. the limit values of the computed E_{ele} for a given basis set) is 0.75 kcal/mol on average, being the maximum value 1.15 kcal/mol for aug-cc-pVDZ. This clearly shows that the computed QM/FQFμ energy values are almost unaffected by the choice of the QM description.

Let us focus on the dependence of E_{ele} on the choice of the basis set. First, we notice that electrostatic energy absolute values increase (of about 5% on average) with adding diffuse functions, that probably due to the spreading of the QM density. The addition of polarization

functions has instead an opposite effect, in fact absolute values decrease of about 17% on average. Such trends are almost constant for all QM descriptions. Calculated E_{ele} obtained by exploiting correlation consistent basis sets are always smaller than Pople-calculated values. Moving from cc-pVDZ to cc-pVQZ, the QM/FQFμ electrostatic energy increases in absolute value, and the same trend is reported if augmented basis sets are considered. aug-cc-PVQZ gives very similar results with respect to 6-311++G**, being the average difference of about 0.5%.

In conclusion, stable values of E_{ele} are obtained by adding both diffuse and polarization functions, so that their inclusion appears mandatory. For this reason, in the following section the 6-31+G* basis set is exploited, being a good compromise between accuracy and computational cost.

4.4 Molecules in aqueous solution

In order to show the applicability of QM/FQFμ to the study of molecular systems, and to investigate on the reliability of its parametrization, in this section the method is applied to four selected molecules in aqueous solution: (R)-Methyloxirane (MOXY), acrolein (ACRO), N-methyl acetamide (NMA) and methanol (MeOH). In the first three molecules solute-solvent Hydrogen Bonding (HB) can occur, however the surrounding water molecules can only act as HB donor. For aqueous MeOH, water molecules can instead act as both H-donor and H-acceptor, due to the presence of the O-H group in solute structure. Therefore, the chosen set of systems can appropriately represent the main solute-solvent interactions which are in place in aqueous solutions.

For each of the selected molecules, we ran classical MD simulations (see Section S4.1 for further details) to sample the phase space. From each MD run, we extracted 10 representative structures. Spheres of 5 Å centered in the oxygen atom in case of MOXY, ACRO, and MeOH, and in the nitrogen atom in case of NMA were cut. Sample final structures are reported in Figure 7, where solute-solvent HBs are sketched. All extracted structures are reported in

Figures S1-S4 in SI. The choice of the spheres' radius is justified by the analysis of the Radial Distribution Functions $g(r)$ (see Section S4.1 in SI), which show that a cutting radius of 5.0 Å guarantees that all water molecules in the first two solvation shells are included. The actual number of water molecules in each of the ten considered snapshots for each system is reported in Table 1.

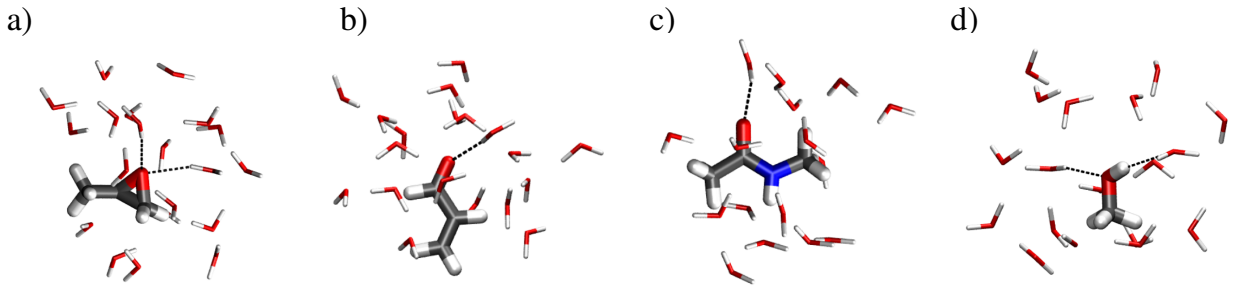

Figure 7: Sample structures obtained by cutting a sphere of 5.0 Å around **a)** (R)-methyloxirane; **b)** acrolein; **c)** N-methyl acetamide; **d)** methanol.

Table 1: Number of water molecules included in each of the ten considered snapshots for each studied molecule in aqueous solution, obtained by using a cutting radius of 5 Å

Structure	MOXY	ACRO	NMA	MeOH
1	22	19	21	26
2	18	23	17	25
3	19	19	19	23
4	19	18	18	19
5	20	19	16	21
6	19	20	17	23
7	20	14	16	18
8	13	19	15	24
9	19	20	16	17
10	20	21	20	25

For each of the extracted structures, solute-solvent E_{ele} was calculated by exploiting both QM/FQ and QM/FQFμ. In case of QM/FQ calculations, three different parametrizations, namely QM/FQ^a,[18] QM/FQ^b[49] and QM/FQ^c[55] were considered. QM/FQ and QM/FQFμ were compared with full-QM electrostatic energies calculated by exploiting SAPT0/6-311++G** (see Figure 8, the corresponding raw data are given in Tables S4-S5 in SI). In both QM/FQ and QM/FQFμ calculations, the QM portion was described at the HF/6-311++G** level,

and the charge constraint in Eq. 21 is imposed so to fix the total charge of the solvent molecules to zero. This implies that Charge Transfer (CT) between different water molecules is allowed. Such a choice is justified by the fact that reference full-QM data implicitly take into account CT between solvent molecules. Additional calculations on the same structures were performed by fixing the total charge of the single MM water to zero; the corresponding results are given in Section S5.4 in SI.

The comparison between polarizable QM/MM and SAPT0 E_{ele} are graphically depicted in Figure 8. RMSD, Maximum Absolute Error (MAE) and Relative Error (RE) on the ten selected structures are reported in Table 2. Let us focus on the results obtained for MOXY in aqueous solution. SAPT0 values range from -17 to -30 kcal/mol, thus showing large electrostatic interactions due to HBs, which are reported for all the ten selected structures (see Figure S1 in SI). QM/FQ^b values are always larger than QM/FQ^a: this is related to the difference between atomic electronegativities of the two parametrizations. Such a difference is larger in FQ^b. On the other hand, QM/FQ^c predicts the greatest absolute E_{ele} values, because polarization is promoted by smaller values of chemical hardnesses. The largest discrepancy between QM/FQ and SAPT0 is observed for the pristine FQ parametrization by Rick et al.,[18] i.e. QM/FQ^a, whereas the best agreement is given by our recent parametrization,[55] i.e. QM/FQ^c (see also Table 2). This is not surprising, because FQ^c was tuned to reproduce the total interaction energy calculated at the CCSD(T) level, whereas FQ^a and FQ^b were set to reproduce bulk water properties (FQ^a, ref.[18]) or QM atomic charges (FQ^b, ref.[49]). As depicted in Figure 8, QM/FQFμ over-performs QM/FQ. This is also confirmed by the data reported in Table 2, where a RMSD of only 1.62 kcal/mol and an RE of 6.47 % are reported. QM/FQFμ E_{ele} are dominated by charge contributions (on average 75%), that in agreement with what has shown above for the water dimer. Raw data of charge/dipoles contributions to QM/FQFμ E_{ele} are reported in Table S4 in SI. To further confirm the quality of QM/FQFμ, the same analysis was applied to a snapshots of MOXY in aqueous solution constructed by using a cutting radius of 7 Å. Such an analysis is discussed in Section S5.7 in SI.

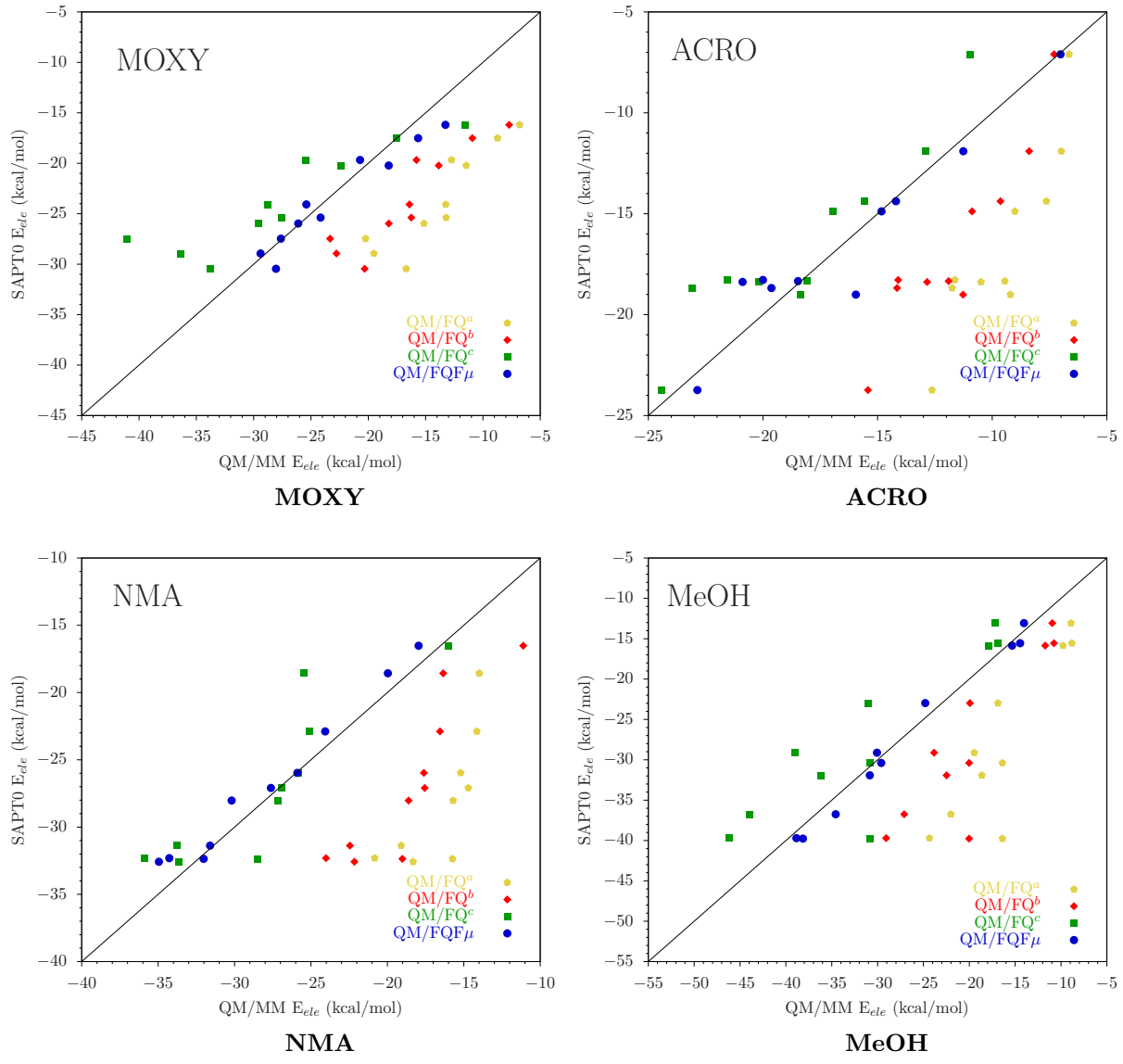

Figure 8: Comparison between calculated QM/FQ^a, QM/FQ^b, QM/FQ^c, QM/FQFμ E_{ele} (HF/6-311++G** level for the QM portion) and SAPT0/6-311++G** data. In case of SAPT0 calculations electrostatic and induction energy contributions are summed up. Raw data are given in Table S5 in SI. All data are reported in kcal/mol.

[a] FQ parametrization taken from Ref.[18]

[b] FQ parametrization taken from Ref.[49]

[c] FQ parametrization taken from Ref.[55]

The same behavior highlighted for MOXY also applies to the other selected molecules (ACRO, MeOH, NMA). In fact, QM/FQFμ always overperforms QM/FQ. This is particularly evident in case of MeOH, where SAPT0 values range from -40 to -15 kcal/mol, thus moving from weak solute-solvent interactions to strong HBs. This is due to the fact the MeOH is the only chosen molecule in which solvent water molecules can act both as H-donor and H-acceptor. Figure 8 clearly shows that at small E_{ele} values all four approaches predict similar energy values, whereas as energy increases, the differences between the methods increases. On the other hand, QM/FQFμ correctly reproduces SAPT0 values in the whole range of energies (i.e. for both weak and strong HBs configurations), as can be seen both from Table 2 and Figure 8, where QM/FQFμ values lie almost perfectly on the diagonal. This can be particularly appreciated from the data shown in the last column of Table 2, which reports a statistical analysis over the whole set of 40 structures. It is also remarkable that QM/FQFμ, as well as all the three QM/FQ parametrizations, give errors with respect to full QM calculation by far lower than what has been recently reported for QM/AMOEBA calculations on different aqueous systems.[92]

To end the discussion, QM/FQFμ charge and dipole contributions for two representative structures of MOXY and MeOH in aqueous solution (structures $MOXY_1$ and MeOH-2 in Figures S1 and S2, given as SI) are analyzed. In Figures 9 and 10, each water molecule is colored as a function of the contribution to E_{ele}. Such an analysis is done according to what has been recently proposed for Functional group-SAPT (FSAPT).[93,94] $MOXY_1$ is characterized by one HB, where a single water molecule acts as H-donor, whereas MeOH-2 is involved in two HBs, in which one water molecules acts as H-donor and a second one as H-acceptor. Figures 9 and 10 clearly show that in both cases HB water molecules give the largest contributions to E_{ele}. However, other water molecules, which are not directly involved in HB with the QM portion, give non-negligible contributions to the total electrostatic energy. This has a practical consequence: in fact, cluster approaches, in which only few, geometrically close, water molecules are included in the QM portion, can inappropriately model solvent

Table 2: Root Mean Squared Deviation (RMSD), Maximum Absolut Error (MAE) and Relative Error (RE) of ten selected structures of MOXY, ACRO, MeOH and NMA in aqueous solution extracted from aqueous solution. SAPT0/6-311++G** E_{ele} values are taken as reference. TOT indicates statistical parameters calculated on all 40 structures extracted from MD runs. RMSD and MAE are given in kcal/mol.
[a] FQ parametrization taken from Ref.[18]
[b] FQ parametrization taken from Ref.[49]
[c] FQ parametrization taken from Ref.[55]

		MOXY	ACRO	NMA	MeOH	TOT
QM/FQ[a]	RMSD	10.02	7.46	11.53	12.66	10.60
	MAE	13.76	11.11	16.62	23.38	23.38
	RE	42.54%	39.72%	40.56%	39.85%	40.67%
QM/FQ[b]	RMSD	7.29	5.38	8.71	9.35	7.83
	MAE	10.14	8.32	13.34	19.75	19.75
	RE	30.85%	28.02%	30.07%	27.09%	29.01%
QM/FQ[c]	RMSD	5.92	2.36	2.96	6.16	4.67
	MAE	13.59	4.41	6.88	9.90	13.59
	RE	19.67%	14.39%	8.79%	19.54%	15.60%
QM/FQFμ	RMSD	1.62	1.44	1.41	1.29	1.45
	MAE	2.92	3.06	2.37	2.18	3.06
	RE	6.47%	5.68%	4.65%	4.72%	5.38%

effects, because such relevant contributions will be most probably neglected.

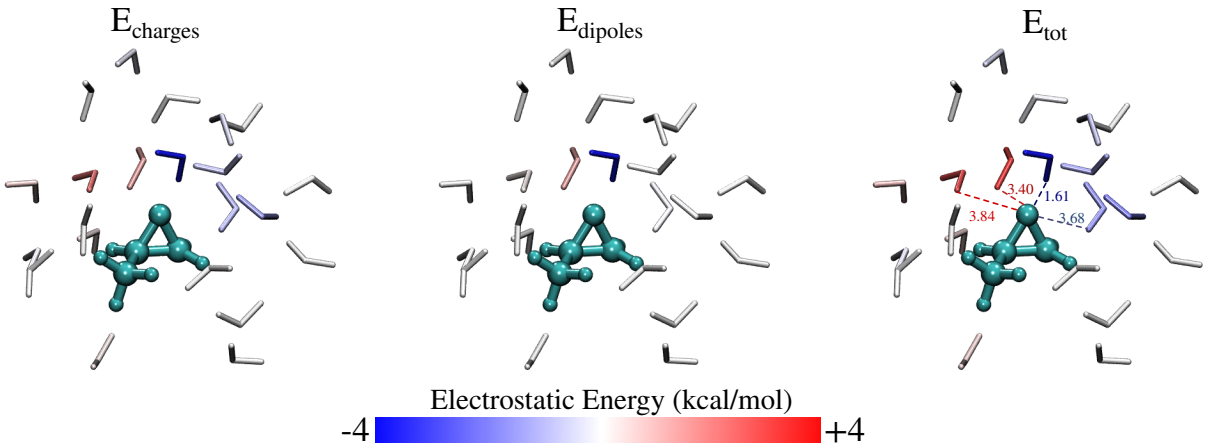

Figure 9: QM/FQFμ electrostatic energy contributions (kcal/mol) for $MOXY_1$. $E_{charges}$ and $E_{dipoles}$ indicate charge and dipole contributions to the total E_{ele}. All atoms in each water molecule are colored according to their contribution. The color maps saturate at ± 4 kcal/mol.

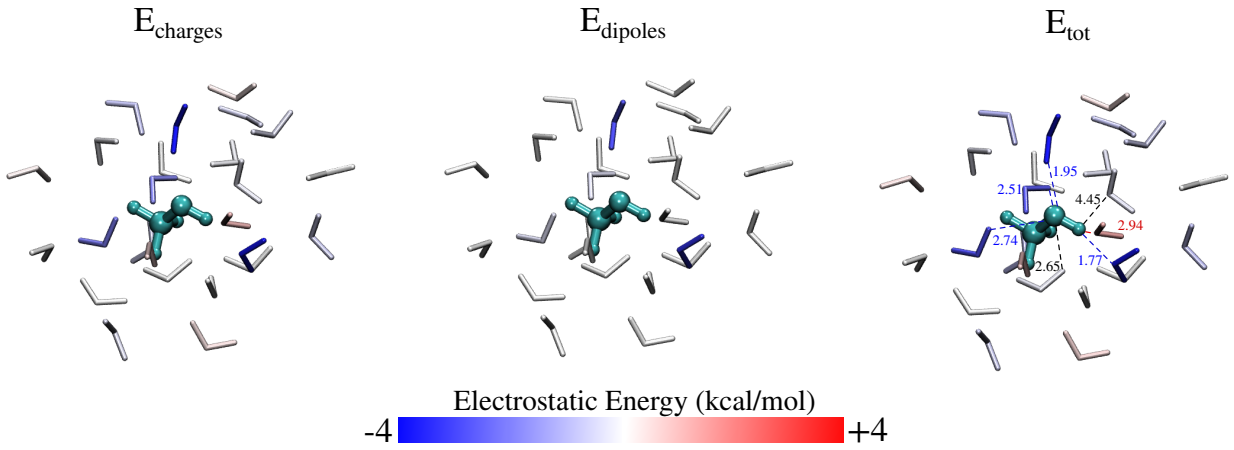

Figure 10: QM/FQFμ electrostatic energy contributions (kcal/mol) for MeOH-2. $E_{charges}$ and $E_{dipoles}$ indicate charge and dipole contributions to the total E_{ele}. All atoms in each water molecule are colored according to their contribution. The color maps saturate at ± 4 kcal/mol.

5 Summary and Conclusions

In this paper, a new polarizable force field, FQFμ, has been proposed and coupled to a QM SCF Hamiltonian. The peculiarity of QM/FQFμ stands in the fact the polarization of the MM portion is modeleed in terms of both charges and dipoles that can vary as a response to the external electric potential/field. From the theoretical point of view, QM/FQFμ approach is an extension of the QM/FQ which we have developed in recent years, REFS in which only fluctuating charges are used to describe the polarization of the environment. Differences and analogies with previously developed methods and a comparison between Drude Oscillators and Fluctuating dipoles has been discussed, pointing out the novelty and the computational features of our approach.

QM/FQFμ has been parametrized in order to reproduce electrostatic energies of aqueous solutions. Then, such an approach has been tested against the reproduction of electrostatic energy of a water dimer as a function of the O-O distance, as well as its total interaction energy. QM/FQFμ has also been coupled with a model that we have recently proposed to account for non-electrostatic energy terms , and it has been shown to appropriately reproduce CCSD(T) equilibrium geometry and the corresponding interaction energy for the same water dimer.

Finally, QM/FQFμ has been applied to the calculation of electrostatic energies of four molecules in aqueous solution. Such molecules were chosen by considering the specific interactions that they can form with the surrounding water molecules (i.e. H-acceptor or H-donor). QM/FQFμ overcomes the limits of QM/FQ, giving a better agreement with reference full QM SAPT0 data. However, all the tested methods are in better agreement with full QM data than what has been shown for QM/AMOEBA on different aqueous systems.[92] The large errors reported for QM/AMOEBA E_{ele} values,[92] have been ascribed to the permanent electrostatic contribution (fixed charges and quadrupoles). Our results seem to show that charge polarization is indeed crucial to lower the errors with respect to full QM values, whereas the inclusion of dipole contributions refines the quality of the results.

To end this discussion we point out that, thanks to its variational formulation, QM/FQFμ can be extended to molecular properties/spectroscopies by following the same strategy which has been proposed by some of us for QM/FQ.[28–30,48,51] Such an extension, as well as model parametrization for non-aqueous environments, will be the topic of future studies.

6 Supporting Information

Equations for FQFμ force field without charge transfer between MM molecules. QM/PQEq model. Details on the parametrization of aqueous solution. Raw data showing the dependence of the electrostatic interaction energy on the level of theory for the water dimer. Details on MD runs of MOXY, ACRO, NMA and MeOH in aqueous solution. Structures of solute-solvent clusters. Electrostatic interaction energies for solute-solvent clusters calculated by exploiting 6-311++G** and 6-31+G* basis sets. Analysis of MOXY-water cluster obtained by exploiting a cutting radius of 7 Å.

7 Acknowledgment

We are thankful for the computer resources provided by the high performance computer facilities of the SMART Laboratory (http://smart.sns.it/). CC gratefully acknowledges the support of H2020-MSCA-ITN-2017 European Training Network "Computational Spectroscopy In Natural sciences and Engineering" (COSINE), grant number 765739. T.G. acknowledges Dr. Franco Egidi (SNS) for helpful discussion.

References

(1) Warshel, A.; Levitt, M. Theoretical studies of enzymic reactions: dielectric, electrostatic and steric stabilization of the carbonium ion in the reaction of lysozyme. *J. Mol. Biol.* **1976**, *103*, 227–249.

(2) Warshel, A.; Karplus, M. Calculation of ground and excited state potential surfaces of conjugated molecules. I. Formulation and parametrization. *J. Am. Chem. Soc.* **1972**, *94*, 5612–5625.

(3) Miertuš, S.; Scrocco, E.; Tomasi, J. Electrostatic interaction of a solute with a continuum. A direct utilizaion of AB initio molecular potentials for the prevision of solvent effects. *Chem. Phys.* **1981**, *55*, 117–129.

(4) Tomasi, J.; Persico, M. Molecular interactions in solution: an overview of methods based on continuous distributions of the solvent. *Chem. Rev.* **1994**, *94*, 2027–2094.

(5) Orozco, M.; Luque, F. J. Theoretical methods for the description of the solvent effect in biomolecular systems. *Chem. Rev.* **2000**, *100*, 4187–4226.

(6) Tomasi, J.; Mennucci, B.; Cammi, R. Quantum mechanical continuum solvation models. *Chem. Rev.* **2005**, *105*, 2999–3094.

(7) Senn, H. M.; Thiel, W. QM/MM methods for biomolecular systems. *Angew. Chem. Int. Ed.* **2009**, *48*, 1198–1229.

(8) Lin, H.; Truhlar, D. G. QM/MM: what have we learned, where are we, and where do we go from here? *Theor. Chem. Acc.* **2007**, *117*, 185–199.

(9) Day, P. N.; Jensen, J. H.; Gordon, M. S.; Webb, S. P.; Stevens, W. J.; Krauss, M.; Garmer, D.; Basch, H.; Cohen, D. An effective fragment method for modeling solvent effects in quantum mechanical calculations. *J. Chem. Phys.* **1996**, *105*, 1968–1986.

(10) Kairys, V.; Jensen, J. H. QM/MM boundaries across covalent bonds: a frozen localized molecular orbital-based approach for the effective fragment potential method. *J. Phys. Chem. A* **2000**, *104*, 6656–6665.

(11) Mao, Y.; Demerdash, O.; Head-Gordon, M.; Head-Gordon, T. Assessing Ion–Water Interactions in the AMOEBA Force Field Using Energy Decomposition Analysis of Electronic Structure Calculations. *J. Chem. Theory Comput.* **2016**, *12*, 5422–5437.

(12) Loco, D.; Polack, É.; Caprasecca, S.; Lagardere, L.; Lipparini, F.; Piquemal, J.-P.; Mennucci, B. A QM/MM approach using the AMOEBA polarizable embedding: from ground state energies to electronic excitations. *J. Chem. Theory Comput.* **2016**, *12*, 3654–3661.

(13) Loco, D.; Cupellini, L. Modeling the absorption lineshape of embedded systems from molecular dynamics: A tutorial review. *Int. J. Quantum Chem.* **2018**, DOI: 10.1002/qua.25726.

(14) Thole, B. T. Molecular polarizabilities calculated with a modified dipole interaction. *Chem. Phys.* **1981**, *59*, 341–350.

(15) Steindal, A. H.; Ruud, K.; Frediani, L.; Aidas, K.; Kongsted, J. Excitation energies in solution: the fully polarizable QM/MM/PCM method. *J. Phys. Chem. B* **2011**, *115*, 3027–3037.

(16) Jurinovich, S.; Curutchet, C.; Mennucci, B. The Fenna–Matthews–Olson Protein Revisited: A Fully Polarizable (TD) DFT/MM Description. *ChemPhysChem* **2014**, *15*, 3194–3204.

(17) Boulanger, E.; Thiel, W. Solvent boundary potentials for hybrid QM/MM computations using classical drude oscillators: a fully polarizable model. *J. Chem. Theory Comput.* **2012**, *8*, 4527–4538.

(18) Rick, S. W.; Stuart, S. J.; Berne, B. J. Dynamical fluctuating charge force fields: Application to liquid water. *J. Chem. Phys.* **1994**, *101*, 6141–6156.

(19) Rick, S. W.; Berne, B. J. Dynamical Fluctuating Charge Force Fields: The Aqueous Solvation of Amides. *J. Am. Chem. Soc.* **1996**, *118*, 672–679.

(20) Cappelli, C. Integrated QM/Polarizable MM/Continuum Approaches to Model Chiroptical Properties of Strongly Interacting Solute-Solvent Systems. *Int. J. Quantum Chem.* **2016**, *116*, 1532–1542.

(21) Stern, H. A.; Kaminski, G. A.; Banks, J. L.; Zhou, R.; Berne, B.; Friesner, R. A. Fluctuating charge, polarizable dipole, and combined models: parameterization from ab initio quantum chemistry. *J. Phys. Chem. B* **1999**, *103*, 4730–4737.

(22) Naserifar, S.; Brooks, D. J.; Goddard III, W. A.; Cvicek, V. Polarizable charge equilibration model for predicting accurate electrostatic interactions in molecules and solids. *J. Chem. Phys.* **2017**, *146*, 124117.

(23) Oppenheim, J. J.; Naserifar, S.; Goddard III, W. A. Extension of the Polarizable Charge Equilibration Model to Higher Oxidation States with Applications to Ge, As, Se, Br, Sn, Sb, Te, I, Pb, Bi, Po, and At Elements. *J. Phys. Chem. A* **2018**, *122*, 639–645.

(24) Mayer, A. Formulation in terms of normalized propagators of a charge-dipole model enabling the calculation of the polarization properties of fullerenes and carbon nanotubes. *Phys. Rev. B* **2007**, *75*, 045407.

(25) Jensen, L. L.; Jensen, L. Atomistic electrodynamics model for optical properties of silver nanoclusters. *J. Phys. Chem. C* **2009**, *113*, 15182–15190.

(26) Rinkevicius, Z.; Li, X.; Sandberg, J. A.; Mikkelsen, K. V.; Ågren, H. A hybrid density functional theory/molecular mechanics approach for linear response properties in heterogeneous environments. *J. Chem. Theory Comput.* **2014**, *10*, 989–1003.

(27) Giovannini, T.; Ambrosetti, M.; Cappelli, C. A polarizable embedding approach to second harmonic generation (SHG) of molecular systems in aqueous solutions. *Theor. Chem. Acc.* **2018**, *137*, 74.

(28) Lipparini, F.; Cappelli, C.; Barone, V. Linear response theory and electronic transition energies for a fully polarizable QM/classical hamiltonian. *J. Chem. Theory Comput.* **2012**, *8*, 4153–4165.

(29) Lipparini, F.; Cappelli, C.; Scalmani, G.; De Mitri, N.; Barone, V. Analytical first and second derivatives for a fully polarizable QM/classical hamiltonian. *J. Chem. Theory Comput.* **2012**, *8*, 4270–4278.

(30) Lipparini, F.; Cappelli, C.; Barone, V. A gauge invariant multiscale approach to magnetic spectroscopies in condensed phase: General three-layer model, computational implementation and pilot applications. *J. Chem. Phys.* **2013**, *138*, 234108.

(31) Giovannini, T.; Del Frate, G.; Lafiosca, P.; Cappelli, C. Effective computational route towards vibrational optical activity spectra of chiral molecules in aqueous solution. *Phys. Chem. Chem. Phys.* **2018**, *20*, 9181–9197.

(32) Jakobsen, S.; Jensen, F. Systematic improvement of potential-derived atomic multipoles and redundancy of the electrostatic parameter space. *J. Chem. Theory Comput.* **2014**, *10*, 5493–5504.

(33) Jakobsen, S.; Jensen, F. Searching the Force Field Electrostatic Multipole Parameter Space. *J. Chem. Theory Comput.* **2016**, *12*, 1824–1832.

(34) Lipparini, F.; Barone, V. Polarizable force fields and polarizable continuum model: a fluctuating charges/PCM approach. 1. theory and implementation. *J. Chem. Theory Comput.* **2011**, *7*, 3711–3724.

(35) Morton, S. M.; Jensen, L. A discrete interaction model/quantum mechanical method for describing response properties of molecules adsorbed on metal nanoparticles. *J. Chem. Phys.* **2010**, *133*, 074103.

(36) Scalmani, G.; Frisch, M. J. Continuous surface charge polarizable continuum models of solvation. I. General formalism. *J. Chem. Phys.* **2010**, *132*, 114110.

(37) Lipparini, F.; Scalmani, G.; Mennucci, B.; Cancès, E.; Caricato, M.; Frisch, M. J. A variational formulation of the polarizable continuum model. *J. Chem. Phys.* **2010**, *133*, 014106.

(38) Löytynoja, T.; Li, X.; Jänkälä, K.; Rinkevicius, Z.; Ågren, H. Quantum mechanics capacitance molecular mechanics modeling of core-electron binding energies of methanol and methyl nitrite on Ag (111) surface. *J. Chem. Phys.* **2016**, *145*, 024703.

(39) Rinkevicius, Z.; Sandberg, J. A.; Li, X.; Linares, M.; Norman, P.; Ågren, H. Hybrid complex polarization propagator/molecular mechanics method for heterogeneous environments. *J. Chem. Theory Comput.* **2016**, *12*, 2661–2667.

(40) Li, X.; Carravetta, V.; Li, C.; Monti, S.; Rinkevicius, Z.; Ågren, H. Optical properties of gold nanoclusters functionalized with a small organic compound: Modeling by an integrated quantum-classical approach. *J. Chem. Theory Comput.* **2016**, *12*, 3325–3339.

(41) Lim, C.-K.; Li, X.; Li, Y.; Drew, K. L.; Palafox-Hernandez, J. P.; Tang, Z.; Baev, A.; Kuzmin, A. N.; Knecht, M. R.; Walsh, T. R.; Swihart, M. T.; Ågren, H.; Prasad, P. N. Plasmon-enhanced two-photon-induced isomerization for highly-localized light-based actuation of inorganic/organic interfaces. *Nanoscale* **2016**, *8*, 4194–4202.

(42) Rappe, A. K.; Goddard III, W. A. Charge equilibration for molecular dynamics simulations. *J. Phys. Chem* **1991**, *95*, 3358–3363.

(43) Lemkul, J. A.; Huang, J.; Roux, B.; MacKerell Jr, A. D. An empirical polarizable force field based on the classical drude oscillator model: development history and recent applications. *Chem. Rev.* **2016**, *116*, 4983–5013.

(44) Geerke, D. P.; Thiel, S.; Thiel, W.; van Gunsteren, W. F. Combined QM/MM molecular dynamics study on a condensed-phase SN2 reaction at nitrogen: The effect of explicitly including solvent polarization. *J. Chem. Theory Comput.* **2007**, *3*, 1499–1509.

(45) Lu, Z.; Zhang, Y. Interfacing ab initio quantum mechanical method with classical Drude osillator polarizable model for molecular dynamics simulation of chemical reactions. *J. Chem. Theory Comput.* **2008**, *4*, 1237–1248.

(46) Boulanger, E.; Thiel, W. Toward QM/MM simulation of enzymatic reactions with the drude oscillator polarizable force field. *J. Chem. Theory Comput.* **2014**, *10*, 1795–1809.

(47) Caprasecca, S.; Jurinovich, S.; Viani, L.; Curutchet, C.; Mennucci, B. Geometry optimization in polarizable QM/MM models: the induced dipole formulation. *J. Chem. Theory Comput.* **2014**, *10*, 1588–1598.

(48) Giovannini, T.; Olszòwka, M.; Egidi, F.; Cheeseman, J. R.; Scalmani, G.; Cappelli, C. Polarizable Embedding Approach for the Analytical Calculation of Raman and Raman Optical Activity Spectra of Solvated Systems. *J. Chem. Theory Comput.* **2017**, *13*, 4421–4435.

(49) Carnimeo, I.; Cappelli, C.; Barone, V. Analytical gradients for MP2, double hybrid functionals, and TD-DFT with polarizable embedding described by fluctuating charges. *J. Comput. Chem.* **2015**, *36*, 2271–2290.

(50) Caprasecca, S.; Cupellini, L.; Jurinovich, S.; Loco, D.; Lipparini, F.; Mennucci, B. A polarizable QM/MM description of environment effects on NMR shieldings: from solvated molecules to pigment–protein complexes. *Theor. Chem. Acc.* **2018**, *137*, 84.

(51) Giovannini, T.; Olszowka, M.; Cappelli, C. Effective Fully Polarizable QM/MM Approach To Model Vibrational Circular Dichroism Spectra of Systems in Aqueous Solution. *J. Chem. Theory Comput.* **2016**, *12*, 5483–5492.

(52) Helgaker, T.; Coriani, S.; Jørgensen, P.; Kristensen, K.; Olsen, J.; Ruud, K. Recent advances in wave function-based methods of molecular-property calculations. *Chem. Rev.* **2012**, *112*, 543–631.

(53) Huang, J.; Simmonett, A. C.; Pickard IV, F. C.; MacKerell Jr, A. D.; Brooks, B. R. Mapping the Drude polarizable force field onto a multipole and induced dipole model. *J. Chem. Phys.* **2017**, *147*, 161702.

(54) Frisch, M. J.; Trucks, G. W.; Schlegel, H. B.; Scuseria, G. E.; Robb, M. A.; Cheeseman, J. R.; Scalmani, G.; Barone, V.; Petersson, G. A.; Nakatsuji, H.; Li, X.; Caricato, M.; Marenich, A. V.; Bloino, J.; Janesko, B. G.; Gomperts, R.; Mennucci, B.; Hratchian, H. P.; Ortiz, J. V.; Izmaylov, A. F.; Sonnenberg, J. L.; Williams-Young, D.; Ding, F.; Lipparini, F.; Egidi, F.; Goings, J.; Peng, B.; Petrone, A.; Henderson, T.; Ranasinghe, D.; Zakrzewski, V. G.; Gao, J.; Rega, N.; Zheng, G.; Liang, W.; Hada, M.; Ehara, M.; Toyota, K.; Fukuda, R.; Hasegawa, J.; Ishida, M.; Nakajima, T.; Honda, Y.; Kitao, O.; Nakai, H.; Vreven, T.; Throssell, K.; Montgomery, J. A., Jr.; Peralta, J. E.; Ogliaro, F.; Bearpark, M. J.; Heyd, J. J.;

Brothers, E. N.; Kudin, K. N.; Staroverov, V. N.; Keith, T. A.; Kobayashi, R.; Normand, J.; Raghavachari, K.; Rendell, A. P.; Burant, J. C.; Iyengar, S. S.; Tomasi, J.; Cossi, M.; Millam, J. M.; Klene, M.; Adamo, C.; Cammi, R.; Ochterski, J. W.; Martin, R. L.; Morokuma, K.; Farkas, O.; Foresman, J. B.; Fox, D. J. Gaussian 16 Revision A.03. 2016; Gaussian Inc. Wallingford CT.

(55) Giovannini, T.; Lafiosca, P.; Chandramouli, B.; Barone, V.; Cappelli, C. *submitted*

(56) Giovannini, T.; Lafiosca, P.; Cappelli, C. A General Route to Include Pauli Repulsion and Quantum Dispersion Effects in QM/MM Approaches. *J. Chem. Theory Comput.* **2017**, *13*, 4854–4870.

(57) Berendsen, H.; van der Spoel, D.; van Drunen, R. GROMACS: A message-passing parallel molecular dynamics implementation. *Comp. Phys. Comm.* **1995**, *91*, 43 – 56.

(58) Lindahl, E.; Hess, B.; van der Spoel, D. GROMACS 3.0: a package for molecular simulation and trajectory analysis. *J. Mol. Model.* **2001**, *7*, 306–317.

(59) Van Der Spoel, D.; Lindahl, E.; Hess, B.; Groenhof, G.; Mark, A. E.; Berendsen, H. J. C. GROMACS: Fast, flexible, and free. *J. Comput. Chem.* **2005**, *26*, 1701–1718.

(60) Hess, B.; Kutzner, C.; van der Spoel, D.; Lindahl, E. GROMACS 4: Algorithms for Highly Efficient, Load-Balanced, and Scalable Molecular Simulation. *J. Chem. Theory Comput.* **2008**, *4*, 435–447.

(61) Lipparini, F.; Egidi, F.; Cappelli, C.; Barone, V. The optical rotation of methyloxirane in aqueous solution: a never ending story? *J. Chem. Theory Comput.* **2013**, *9*, 1880–1884.

(62) Giovannini, T.; Macchiagodena, M.; Ambrosetti, M.; Puglisi, A.; Lafiosca, P.; Lo Gerfo, G.; Egidi, F.; Cappelli, C. Simulating vertical excitation energies of solvated dyes: From continuum to polarizable discrete modeling. *Int. J. Quantum Chem.* **2018**, e25684.

(63) Kitaura, K.; Morokuma, K. A new energy decomposition scheme for molecular interactions within the Hartree-Fock approximation. *Int. J. Quantum Chem.* **1976**, *10*, 325–340.

(64) Morokuma, K.; Kitaura, K. *Chemical applications of atomic and molecular electrostatic potentials*; Springer, 1981; pp 215–242.

(65) Schmidt, M. W.; Baldridge, K. K.; Boatz, J. A.; Elbert, S. T.; Gordon, M. S.; Jensen, J. H.; Koseki, S.; Matsunaga, N.; Nguyen, K. A.; Su, S.; Windus, T. L.; Dupuis, M.; Montgomery, J. A. General atomic and molecular electronic structure system. *J. Comput. Chem.* **1993**, *14*, 1347–1363.

(66) Gordon, M. S.; Schmidt, M. W. *Theory and Applications of Computational Chemistry: the first forty years*; Elsevier, 2005; pp 1167–1189.

(67) Szalewicz, K. Symmetry-adapted perturbation theory of intermolecular forces. *WIRES: Comput. Mol. Sci.* **2012**, *2*, 254–272.

(68) Hohenstein, E. G.; Sherrill, C. D. Wavefunction methods for noncovalent interactions. *WIRES: Comput. Mol. Sci.* **2012**, *2*, 304–326.

(69) Parrish, R. M.; Burns, L. A.; Smith, D. G. A.; Simmonett, A. C.; DePrince, A. E.; Hohenstein, E. G.; Bozkaya, U.; Sokolov, A. Y.; Di Remigio, R.; Richard, R. M.; Gonthier, J. F.; James, A. M.; McAlexander, H. R.; Kumar, A.; Saitow, M.; Wang, X.; Pritchard, B. P.; Verma, P.; Schaefer, H. F.; Patkowski, K.; King, R. A.; Valeev, E. F.; Evangelista, F. A.; Turney, J. M.; Crawford, T. D.; Sherrill, C. D. Psi4 1.1: An Open-Source Electronic Structure Program Emphasizing Automation, Advanced Libraries, and Interoperability. *J. Chem. Theory Comput.* **2017**, *13*, 3185–3197.

(70) Kratz, E. G.; Walker, A. R.; Lagardère, L.; Lipparini, F.; Piquemal, J.-P.; Andrés Cisneros, G. LICHEM: A QM/MM program for simulations with multipolar and polarizable force fields. *J. Comput. Chem.* **2016**, *37*, 1019–1029.

(71) Jensen, J. H.; Gordon, M. S. An approximate formula for the intermolecular Pauli repulsion between closed shell molecules. *Mol. Phys.* **1996**, *89*, 1313–1325.

(72) Jensen, J. H.; Gordon, M. S. An approximate formula for the intermolecular Pauli repulsion

between closed shell molecules. II. Application to the effective fragment potential method. *J. Chem. Phys.* **1998**, *108*, 4772–4782.

(73) Tkatchenko, A.; Scheffler, M. Accurate molecular van der Waals interactions from ground-state electron density and free-atom reference data. *Phys. Rev. Lett.* **2009**, *102*, 073005.

(74) Tkatchenko, A.; Romaner, L.; Hofmann, O. T.; Zojer, E.; Ambrosch-Draxl, C.; Scheffler, M. Van der Waals interactions between organic adsorbates and at organic/inorganic interfaces. *MRS bulletin* **2010**, *35*, 435–442.

(75) Tkatchenko, A.; DiStasio Jr, R. A.; Car, R.; Scheffler, M. Accurate and efficient method for many-body van der Waals interactions. *Phys. Rev. Lett.* **2012**, *108*, 236402.

(76) Hermann, J.; DiStasio, R. A.; Tkatchenko, A. First-Principles Models for van der Waals Interactions in Molecules and Materials: Concepts, Theory, and Applications. *Chem. Rev.* **2017**, *117*, 4714–4758.

(77) Curutchet, C.; Cupellini, L.; Kongsted, J.; Corni, S.; Frediani, L.; Steindal, A. H.; Guido, C. A.; Scalmani, G.; Mennucci, B. Density-Dependent Formulation of Dispersion–Repulsion Interactions in Hybrid Multiscale Quantum/Molecular Mechanics (QM/MM) Models. *J. Chem. Theory Comput.* **2018**, *14*, 1671–1681.

(78) Egidi, F.; Carnimeo, I.; Cappelli, C. Optical rotatory dispersion of methyloxirane in aqueous solution: assessing the performance of density functional theory in combination with a fully polarizable QM/MM/PCMapproach. *Opt. Mater. Express* **2015**, *5*, 196–209.

(79) Jacquemin, D.; Moore, B.; Planchat, A.; Adamo, C.; Autschbach, J. Performance of an optimally tuned range-separated hybrid functional for 0–0 electronic excitation energies. *J. Chem. Theory Comput.* **2014**, *10*, 1677–1685.

(80) Perdew, J. P.; Burke, K.; Ernzerhof, M. Generalized Gradient Approximation Made Simple. *Phys. Rev. Lett.* **1997**, *78*, 1396–1396.

(81) Becke, A. D. Density-functional thermochemistry. V. Systematic optimization of exchange-correlation functionals. *J. Chem. Phys.* **1997**, *107*, 8554–8560.

(82) Schmider, H. L.; Becke, A. D. Optimized density functionals from the extended G2 test set. *J. Chem. Phys.* **1998**, *108*, 9624–9631.

(83) Perdew, J. P.; Ruzsinszky, A.; Csonka, G. I.; Constantin, L. A.; Sun, J. Workhorse Semilocal Density Functional for Condensed Matter Physics and Quantum Chemistry. *Phys. Rev. Lett.* **2009**, *103*, 026403.

(84) Becke, A. D. Density-functional exchange-energy approximation with correct asymptotic behavior. *Phys. Rev. A* **1988**, *38*, 3098–3100.

(85) Zhao, Y.; Truhlar, D. G. The M06 suite of density functionals for main group thermochemistry, thermochemical kinetics, noncovalent interactions, excited states, and transition elements: two new functionals and systematic testing of four M06-class functionals and 12 other functionals. *Theor. Chem. Acc.* **2008**, *120*, 215–241.

(86) Adamo, C.; Barone, V. Toward reliable density functional methods without adjustable parameters: The PBE0 model. *J. Chem. Phys.* **1999**, *110*, 6158–6170.

(87) Becke, A. D. Density-functional thermochemistry. III. The role of exact exchange. *J. Chem. Phys.* **1993**, *98*, 5648–5652.

(88) Peverati, R.; Truhlar, D. G. Communication: A global hybrid generalized gradient approximation to the exchange-correlation functional that satisfies the second-order density-gradient constraint and has broad applicability in chemistry. *J. Chem. Phys.* **2011**, *135*, 191102.

(89) Adamo, C.; Barone, V. Exchange functionals with improved long-range behavior and adiabatic connection methods without adjustable parameters: The mPW and mPW1PW models. *J. Chem. Phys.* **1998**, *108*, 664–675.

(90) Yanai, T.; Tew, D. P.; Handy, N. C. A new hybrid exchange–correlation functional using the Coulomb-attenuating method (CAM-B3LYP). *Chem. Phys. Lett.* **2004**, *393*, 51–57.

(91) Dunning Jr, T. H. Gaussian basis sets for use in correlated molecular calculations. I. The atoms boron through neon and hydrogen. *J. Chem. Phys.* **1989**, *90*, 1007–1023.

(92) Mao, Y.; Shao, Y.; Dziedzic, J.; Skylaris, C.-K.; Head-Gordon, T.; Head-Gordon, M. Performance of the AMOEBA water model in the vicinity of QM solutes: A diagnosis using energy decomposition analysis. *J. Chem. Theory Comput.* **2017**, *13*, 1963–1979.

(93) Parrish, R. M.; Parker, T. M.; Sherrill, C. D. Chemical assignment of symmetry-adapted perturbation theory interaction energy components: the functional-group SAPT partition. *J. Chem. Theory Comput.* **2014**, *10*, 4417–4431.

(94) Parrish, R. M.; Thompson, K. C.; Martínez, T. J. Large-Scale Functional Group Symmetry-Adapted Perturbation Theory on Graphical Processing Units. *J. Chem. Theory Comput.* **2018**, *14*, 1737–1753.